Degradation Estimation and Prediction of Electronic Packages Using Data-Driven Approach

Alexandru Prisacaru, Przemyslaw Gromala, *Senior Member, IEEE*, Bongtae Han, and Guo Qi Zhang, *Fellow, IEEE*

***Abstract*—Recent trends in automotive electronics such as automated driving will increase the number and complexity of electronics used in safety-relevant applications. Applications in logistics or ridesharing will require a specific year of service rather than the conventional mileage usage. Reliable operations of the electronic systems must be assured at all times, regardless of the usage condition. A more dynamic and on-demand way of assuring the system availability will have to be developed. This article proposes a thermomechanical stress-based prognostics method as a potential solution. The goal is achieved by several novel advancements. On the experimental front, a key microelectronics package is developed to directly apply the prognostics and health management concept using a piezoresistive silicon-based stress sensor. Additional hardware for safe and secure data transmission and data processing is also developed, which is critically required for recording *in situ* and real-time data. On the data management front, proper data-driven approaches have to be identified to handle the unique dataset from the stress sensor employed in this study. The approaches effectively handle the massive amount of data that reveals the important information and automation of the prognostic process and thus to be able to detect, classify, locate, and predict the failure. The statistical techniques for diagnostics and the machine learning algorithms for health assessment and prognostics are also determined to implement the approaches in a simple, fast, but accurate way within the capacity of limited computing power. The proposed prognostics approach is implemented with actual microelectronics packages subjected to harsh accelerated testing conditions. The results corroborate the validity of the proposed prognostics approach.**

***Index Terms*—Data-driven, electronic packages, machine learning (ML), piezoresistive stress sensor, prognostics and health management, recurrent neural network (RNN).**

Manuscript received September 14, 2020; revised January 6, 2021 and February 10, 2021; accepted March 6, 2021. Date of publication March 30, 2021; date of current version December 6, 2021. This work was supported by the Federal Government of Germany, Framework Program for Research and Innovation 2016–2020 Microelectronics—Innovation Drivers of Digitalization through Project smartSTAR under Grant 16ES0965. *(Corresponding author: Alexandru Prisacaru.)*

Alexandru Prisacaru and Przemyslaw Gromala are with the Division of Automotive Electronics, Robert Bosch GmbH, 72762 Reutlingen, Germany (e-mail: alexandru.prisacaru@de.bosch.com; PrzemyslawJakub.Gromala@de.bosch.com).

Bongtae Han is with the College of Computer Mathematical and Natural Sciences, University of Maryland, College Park, MD 20742 USA (e-mail: bthan@umd.edu).

Guo Qi Zhang is with the Delft University of Technology, 2628 CD Delft, The Netherlands (e-mail: G.Q.Zhang@tudelft.nl).

Color versions of one or more figures in this article are available at https://doi.org/10.1109/TIE.2021.3068681.

Digital Object Identifier 10.1109/TIE.2021.3068681

I. Introduction

MICROELECTRONICS packages are composed of multilayer dissimilar materials with complex geometries. These composite interfaces, corners, and edges are subjected to various loading conditions during manufacturing as well as operation [1]. The packaging technologies are used to protect sensitive electronic components for various applications such as telecommunication, automotive, and aerospace.

During operation, the internal stress state changes due to the coefficient of thermal expansion (CTE) mismatch among the materials used in the package as well as the stress concentrations at material discontinuities, which can cause thermomechanical failures. According to [2], these failures account for more than 65% of the total failures in electronics.

Prognostics is the process of predicting a future state (of reliability) based on current and historic conditions. Prognostics and health management (PHM) is a method that permits the reliability of a system to be evaluated in its actual life-cycle conditions to determine the advent of failure and mitigate the system risks [3]. One of the ways to perform prognostics is to measure the mechanical stresses directly using a stress sensor. Such a sensor was originally developed to measure the manufacturing stresses [4], but was extended successfully to various applications, including transfer molding [5], packaging [6], molding relaxation [7], prognostics [8], [9], and condition monitoring [10], [11]. In [12], the sensor was packaged in a Quad Flat No-leads (QFN), and the stress field has been recorded after the damage. Although the damage was observed in the stress field, the limitation is that the delamination is imposed *a priori*. Delamination was also reported in [13]. A flip chip as an application was used during the reliability testing. While the delamination was successfully monitored, the delamination happened exactly at the sensor interface, and only 11 measuring cells were used.

0278-0046 © 2021 IEEE. Personal use is permitted, but republication/redistribution requires IEEE permission.
See https://www.ieee.org/publications/rights/index.html for more information.

Authorized licensed use limited to: University of Maryland College Park. Downloaded on March 07,2022 at 11:42:47 UTC from IEEE Xplore. Restrictions apply.

In the previous related paper [8], delamination was successfully detected in an overmolded electronic unit test vehicle (TV) using such a stress sensor. The propagation of the delamination was also successfully monitored. Yet, the available experimental data were limited (the delamination was *a priori* imposed), and delamination was correlated with stress data only qualitatively. This is the motivation of the current article. Algorithms and techniques for automated degradation estimation and prediction for electronic packages using mechanical stress have not been reported yet.

Significantly more data are required to predict the health condition quantitatively. They should be collected from multiple samples, and each sample should provide continuous stress signals from the healthy state to the state of complete failure. The previous approach by which the data are handled manually using a degradation model becomes simply unfeasible for such a large amount of data [8]. For example, raw data for each sample go up to 2.5 GB for 2500 cycles. A finite-element method validation of the current experiments used in this article was performed in [14]. A classical backpropagation neural network was used to estimate the degradation. The results showed that an improved model is needed.

In this article, the stress-based PHM capability is extended into a quantitative domain, where accurate prediction of remaining useful life (RUL) becomes possible. The goal is achieved by several major novel advancements:

1) nondestructive and *in situ* detection of the delamination during accelerated testing;
2) successful classification of the data obtained from two different failure modes;
3) quantitative estimation of delamination location, state of health, and degradation of automotive electronic packages using machine learning (ML).

The rest of this article is organized as follows. In Section II, the general PHM framework adopted in this study is introduced. An experimental setup and a TV are described in Section III. Results from actual tests and various strategies for evaluation and processing the data are presented in Section IV. Diagnostics by means of failure detection, location, and classification is shown in Section V. Section VI presents the health assessment and prognostics. Finally, Section VII concludes this article.

II. Methodology

In this section, the PHM framework is presented. The fundamentals of the methods used in the methodology are also discussed. The workflow of the PHM methodology is described in Fig. 1.

One of the most important aspects in PHM is the sensor data selection, as it has to be sensitive to a damage of interest. A piezoresistive silicon-based stress sensor was employed in this study, due to its direct connection to any physical changes in the package [15]. The stresses are calculated based on the two measured quantities: 1) the stresses determined from pMOS and nMOS current values and 2) the temperature determined

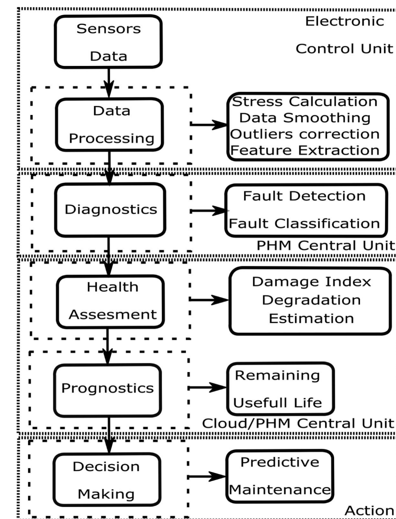

Fig. 1. Algorithm flowchart that depicts the workflow of the PHM methodology and the corresponding hardware.

from the voltages. Both pMOS and nMOS (p and n channel MOSFETs) transistors are used for the stress difference $D(\sigma) = \sigma_{XX} - \sigma_{YY}$ calculation and shear stress σ_{XY}, respectively. These values are calculated from the following relationship:

$$D(\sigma) = \sigma_{xx} - \sigma_{yy} = \frac{1}{\pi_{44}^{p}} \frac{I_{\text{OUT}} - I_{\text{IN}}}{I_{\text{OUT}} + I_{\text{IN}}} \tag{1}$$

$$\sigma_{xy} = \frac{1}{\pi_{11}^{n} - \pi_{12}^{n}} \frac{I_{\text{OUT}} - I_{\text{IN}}}{I_{\text{OUT}} + I_{\text{IN}}} \tag{2}$$

where π_{11}, π_{12}, and π_{44} are the piezoresistive coefficients of silicon, and I_{IN} and I_{OUT} are the currents measured at the input and output of the sensor, respectively. These data are then passed through a preprocessing step that removes outliers, smoothens the data, and extracts the relative stresses caused by the temperature change. More details about the theoretical background of the stress sensor can be found in [16], and the fundamentals of how to use such sensor in reliability are described in detail in [15].

An acquisition unit (AU) is utilized to acquire the sensor signals, and the second unit is to process and transmit the data (PHM central unit). Through this platform, the data from the sensors are collected, processed, and transmitted to a cloud or a database server.

A visualization metric is used to observe any change in the sensor data that might indicate a shift from the normal operation. To automate this process, a failure detection algorithm is used in parallel to check if the stress data are within the threshold. Most of the failure detection algorithms can be easily biased by some unknown operating conditions or some other unexpected events. Therefore, a visualization metric is necessary as a robust measure. After the failure is recognized, a diagnostic tool is used to classify the data in groups, which are subsequently assigned to a certain physical quantity. An algorithm for degradation

Authorized licensed use limited to: University of Maryland College Park. Downloaded on March 07,2022 at 11:42:47 UTC from IEEE Xplore. Restrictions apply.

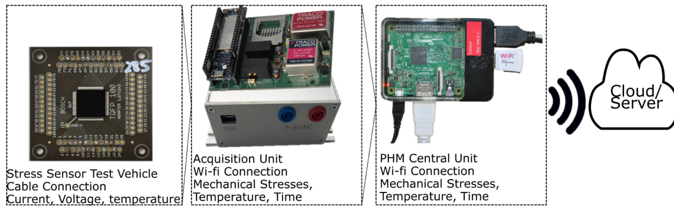

Fig. 2. Data flow representation. On each chart, the electronic unit, the connection, and the data output are described.

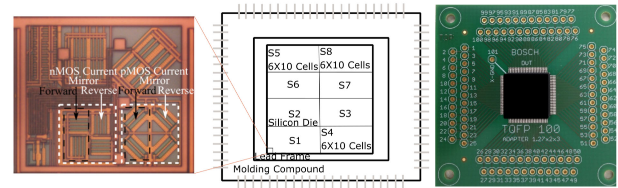

Fig. 3. Test vehicle. Eight stress sensors encapsulated in a TQFP package mounted on a PCB. It indicates the sensor location, definition, and the number of measuring cells.

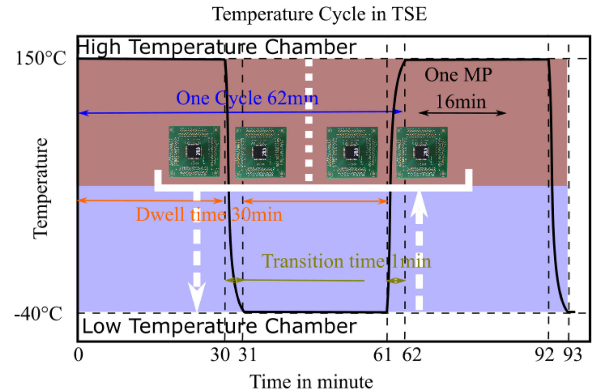

Fig. 4. Temperature cycle duration. The transition time and the dwell time are briefly specified.

estimation and prediction is then applied to quantitatively assess the failure.

Simple, fast, and accurate models are chosen in this methodology. The process of choosing the algorithms is made based on the performance evaluation in comparison with the failure analysis. A scanning acoustic microscope (SAM) and cross-sectioning are used collectively for the required detailed failure analysis.

A. AU and Central PHM Unit

As mentioned earlier, the piezoresistive silicon-based stress sensor was developed originally for measuring stresses during the manufacturing processes [17]. A dedicated AU is required to steer the sensor and to successfully record the data. The first AU was developed together with the sensor [18], but its large size and the small number of sensors for simultaneous measurements made it impractical for *in situ* applications. The second AU developed by Palczynska *et al.* [19] made the *in situ* measurements possible by scaling down the unit with a 12-V power source. In addition, a multiplexer was added to increase the maximum number of sensors. More advancements are required to cope with other challenging issues encountered in actual applications: the large amount of data, further miniaturization, data remote access, computing power, and long running experiments. Such a system is depicted in Fig. 2.

The newly developed AU consists of Arduino Yun Mini board as well as a custom-designed board. The former is used to control and readout the sensor and the latter to power and steer the sensor. The Arduino board is equipped with a microcontroller and a microprocessor that sustains the Wi-Fi shield.

III. Experimental Setup and Test Vehicle

One critical failure mechanism of semiconductor packages is the loss of adhesion at interfaces causing delamination. Failure modes that are caused by delamination are the passivation damage, wire-bond degradation, intermittent electrical failure, and popcorn cracking.

A. Test Vehicle

The TV used in this study is a thin-quad flat package (TQFP) mounted on a printed circuit board (PCB). A TQFP encapsulates eight sensors on a single die, as depicted in Fig. 3. Each sensor consists of 60 measurement cells in a 6×10 matrix, and every each cell contains the pMOS and nMOS transistors, as shown in Fig. 3. Seven TVs fabricated from two different molding compounds are used in the experiment. The TVs are numbered as MCi_j, where i is the molding compound and j is the number of samples.

The TVs use preoxidized leadframe, which significantly reduces the interface strength between the molding compound and the copper pad. It is expected that the delamination process starts at different times for $MC1$ and $MC2$.

Temperature shock (TS) testing is used for damage acceleration in the study. A TS equipment used in the experiment contains two separate chambers, which are preset at different temperatures. The temperature profile consists of -40 and $150\ ^\circ$C, as shown in Fig. 4. Considering the amount of time needed for the AU to acquire one measurement point (MP), every cycle produces two or three MPs. Several samples are placed on the basket, and the signal wires are taken out though the middle hollow cylinder, which is used for the basket movement. The transition between temperatures is short due to the mobility of the basket (according to Fig. 4). The stresses inflicted to the samples in this type of chamber are larger than in a regular thermal chamber due to the fast transition. The temperature difference between the TV and the chamber is initially high, imposing extra stresses.

IV. Experimental Results

Repeated loading causes accumulated fatigue damage, leading to cracks and rupture. It is generally understood that exposing

Authorized licensed use limited to: University of Maryland College Park. Downloaded on March 07,2022 at 11:42:47 UTC from IEEE Xplore. Restrictions apply.

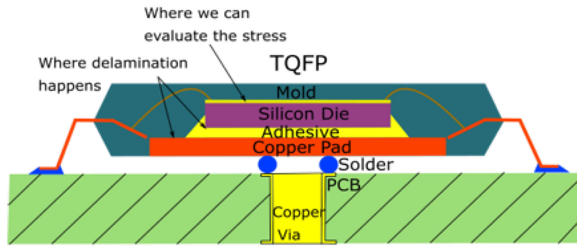

Fig. 5. Package on PCB cross section. It shows the main elements of the package and illustrates where the stresses are measured and, at the same time, where the delamination usually occurs.

surface-mount plastic parts to high-temperature reflow profiles can generate package failures if delamination is present. Fig. 5 depicts where the delamination occurs and where the stresses are measured in a typical package.

Two experiments were performed in two separate TS chambers. The temperature profile used in the experiment is described in Fig. 4. In the first experiment, the TVs were cycled for 750 TS cycles with a dwell time of 30 min, and in the second experiment, for 1600 TS cycles with a dwell time of 40 min.

The stress data were continuously recorded during TS cycling. The data from the TV stress sensor were captured with the AU by a cable connection, which was placed outside the chamber. The AU was sending the data to the Wi-Fi Console, followed by the Raspberry Pi to collect these data from the Console and save it. A simple graphical interface was used in Raspberry Pi to check the status of the experiments and the stresses in real time. At every 50 MPs, the data were sent to the cloud server. The possibility of accessing the Raspberry Pi with a monitor, remote access, or a smartphone provides flexibility and better control over the experiments.

The raw data gathered from the experiment were composed of the high-precision physical measures of voltages and currents from each individual cell of the TV and the times when the measurements were performed. By themselves, these measures do not provide any valuable insight into the matter of this study. All these data are contained in a single dataset.

A. Data Preprocessing

The stress difference is computed using (1) and (2), with the corresponding current values from the raw dataset. The temperatures are calculated from the measured voltages, and the time for measurements is extracted from raw data. All calculation steps are described in Table I.

Each step is summarized as follows.

1) *Step 1:* DIF stores the stress difference values of each cell per MP, TEM stores the temperature values of each cell per MP, and TIME stores the time at the beginning of the recording of each MP.
2) *Step 1:* Data cleaning techniques usually include detecting N/A values, outliers, and gaps on the data. It is always the first step in data preprocessing [20], [21]. These values are shown in Fig. 6.

TABLE I
DATA PROCESSING

Input: Sensors Data $I_{OUT}, I_{IN}, V, Time$
Output: Relative stress difference, Temp, Time per Cycle:
$D(\sigma)_{ij} = (\sigma_{xx} - \sigma_{yy})^{ij}_{T=-40^\circ C} - (\sigma_{xx} - \sigma_{yy})^{ij}_{T=150^\circ C}$
1. Stress Difference, temperature and time calculation:
DIF$_{ik}$, TEM$_{ik}$ and TIME$_k$
2. Data cleaning: Calibration of temperatures and outliers
correction: $NAT \in [-1, 1]$, $N/A = 0$
3. Labeling: Temperature classification.
$TemCat_k =$ "$high(150^\circ)$" $\forall NAT_k \in [1.00, 0.98]$
$TempCat_k =$ "$low(-40^\circ)$" $\forall NAT_k \in [-0.98, 1.00]$
$TempCat_k =$ "$undefined$" $\forall NAT_k \in [0.98, -0.98]$
4. Smoothing: Sliding Window
$DIF_{ik} = \sqrt{\frac{1}{w} \sum_{k=1}^{k=w} (DIF_k - \overline{DIF})^2}$
5. Space Transformation: Cycle space; One value per cycle
$(\sigma_{xx} - \sigma_{yy})^{ij} = T_j[(DIF_{ik})]$
$*i = 1, 2, ..., n$ and $n =$ total number of cells
$*j = 1, 2, ..., m$ and $m =$ number of cycles
$*k = 1, 2, ..., p$ and $p =$ total number of measurement points

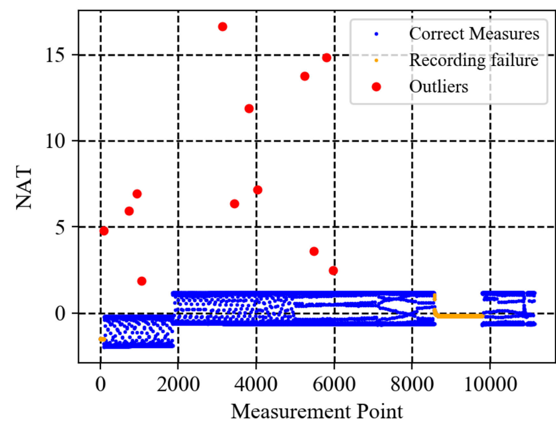

Fig. 6. Normalized average temperature (NAT) of sensor 3. The temperature is calculated at each cell position and then averaged in one value. The jump in the scaling data is represented by a stop and start of the experiment. The orange data is explained by a pause in the chamber operation.

3) *Step 1:* Handling of outliers on the temperature feature is straightforward as the final distribution along the NAT axis is known. All values of NAT must fall around +1 and −1 after normalization. Values exceeding these thresholds are data transmission errors and are taken out.
4) *Step 1:* DIF must pass now through a filtering process to reduce sources of noise [21]. Not all data will be relevant on a later step, so only data points classified as "high" and "low" will be filtered for speeding up the process. A window filter of three data points is used. The value of the data point at the center of the window is replaced by the average of its sides if the standard deviation (SD) surpasses a fixed threshold of 1.1.
5) *Step 1:* After the filtering process, two or three measures on each peak or dwell time of the temperature cycle are kept. A transformation is performed reducing every

Authorized licensed use limited to: University of Maryland College Park. Downloaded on March 07,2022 at 11:42:47 UTC from IEEE Xplore. Restrictions apply.

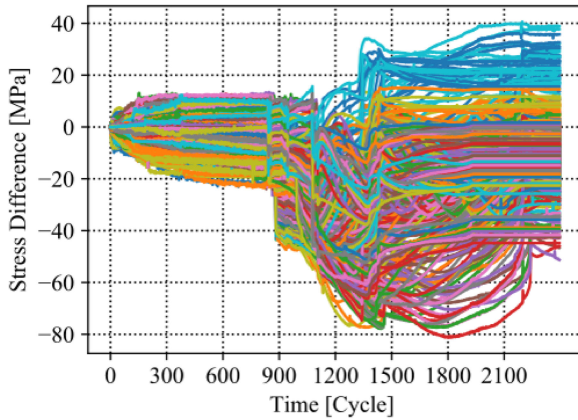

Fig. 7. $MC1_1$ TV 480 stress difference sensing cells representation during the experiment.

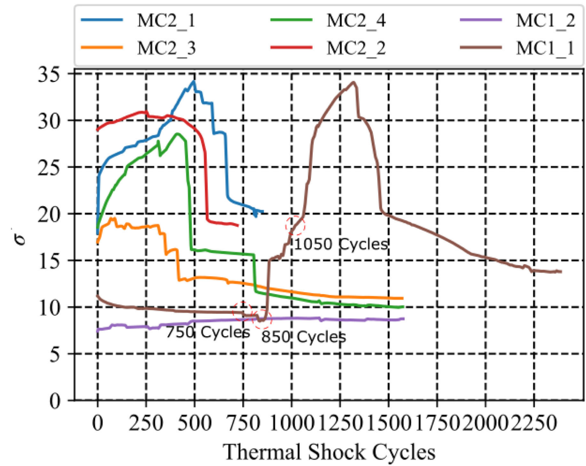

Fig. 8. Visualization metric. The sum of absolute stress value change divided by the number of cells in cycle time for $MC1$ and $MC2$.

sequence of MPs to just one point, whose value is the average of the original points.

The sensor dataset has been finally reduced to an understandable form. The dimensions have been reduced to include one unique signal per cell on the sensor that shows the stress difference variation between the peak low temperature and the peak high temperature of each of the TS cycles the TV was exposed to. Fig. 7 depicts such a unique signal per cell of all 480 measuring locations. After applying the data processing to the datasets obtained from the experiment, the visualization of one single signal per cell is possible, representing the relative values of stresses, by subtracting the residual stresses. These new values are representing the stress given by the temperature change $\Delta T = 190°\text{C}$.

B. Visualization Metric

It is reasonable to assume that the delamination processes at both the molding compound/copper pad interface and the silicon die/die attach interface can alter the stress distribution over the surface of the silicon die. Even after the stress transformation into one single value per cell and cycle, it is still difficult to analyze the data in the form of 480 cells (see Fig. 7). A certain load metric, which well represents the effect of CTE mismatch and integrates data from the 480 cells, is required to represent the applied loading [22].

A load metric can be defined using the stress signals from all 480 cells as

$$\sigma^* = \frac{\sum_{i=1}^{480} |D(\sigma)_i|}{480}. \tag{3}$$

In this manner, the data from 480 parameters were reduced to a single value, which makes analyzing the stress feasible. Using this procedure, the stress response for the whole die can be visualized, as depicted in Fig. 8. Sudden increase or sudden drop in stress indicates delamination initiation and propagation in the package. It is important to recall that the crack propagation rate is inversely proportional to the rate of the interface stiffness change, i.e., the stress rate changes with the crack propagation rate.

Visualizing the data from the TV $MC1_1$ in Fig. 8, the following observations are made.

1) Between 0 and 750 TS cycles, the stresses have a relatively constant value. Small changes are observed due to the moisture release and relaxation effects. This can also be attributed to the effect of aging-induced oxidization on the package stress that has been reported recently [23].
2) Around 850 TS cycles, there is a small drop followed by a large sudden increase in the stress, indicating a significant change in the package structure.
3) Afterward, the stresses change at a slow rate but still follow the same trend of increasing for approximately additional 500 cycles until reaching the maximum value. This indicates further changes in the structure.
4) From 1350 TC cycles onward, the stresses increase initially at a fast rate, but the rate becomes slow. This is an indication that the changes inside the package reach the ending phase.

The overall behavior of the stresses in $MC1_2$ TV is constant during the TS, indicating no changes in the package structure. In comparison with $MC1_1$, the stress behavior does not show any initial changes linked to the moisture and also no sudden drops. There are only few small changes caused by interruption of the experiment. The visualization metric of all samples is depicted in Fig. 8. Based on these initial plots, it is observed that all other samples $MC2_1$, $MC2_2$, $MC2_3$, and $MC2_4$ have some initial delamination. It is speculated that the interface toughness between the molding compound and the copper pad in the case of $MC2$ is smaller than that in the case of $MC1$. The next subsection explains how the changes shown by the visualization metric are connected to the delamination.

C. Failure Analysis

Using the visualization metric, a change in the sensor data was observed, indicating a shift from the normal conditions. These observations are confirmed by the physical failure and

Authorized licensed use limited to: University of Maryland College Park. Downloaded on March 07,2022 at 11:42:47 UTC from IEEE Xplore. Restrictions apply.

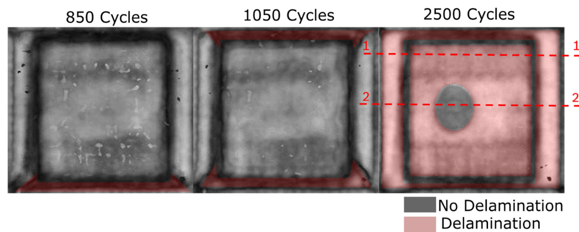

Fig. 9. SAM of $MC1_1$ during and after the experiment. Delamination is detected and is depicted in red areas. Two cross sections are performed at the end of the experiment.

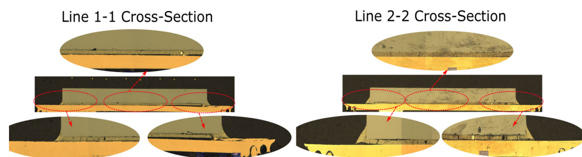

Fig. 10. Cross-section failure analysis of $MC1_1$ along lines 1-1 and 2-2. Crack is present at the interface between molding compound/copper pad and die attach/copper pad along the entire cross section for line 1-1, except the middle part in line 2-2.

the location documented by SAM images and cross-sectional images.

The relative stress difference was correlated with delamination using SAM images. The SAM images taken at various stages are shown in Fig. 9. The samples were taken out from the TS chamber for taking SAM images. The cables were removed for SAM imaging, and they were resoldered to the samples before placing them back in the TS chambers. The state of the package $MC1_1$ before and after 750 TS does not show any delamination (see Fig. 9). The significant change in the stress is observed around 850 cycles. A SAM analysis was performed again at 850 cycles, and the image is shown in Fig. 9. The image clearly shows that delamination started at the bottom of the package, which correlates well with the sudden increase in stress shown in Fig. 8 for $MC1_1$.

The same sample was tested again by the SAM after additional 200 TS cycles. The image shows that a new delamination started on the other side, while the first delamination propagated. The SAM image confirmed the crack growth. The stress history in Fig. 8 (the maximum stress levels at that specific point in time) also corroborates this.

At the end of the experiment, at around 2500 TS cycles, another SAM analysis was performed. The image clearly shows that delamination occurred everywhere except for a small area at the center (see Fig. 9). To further validate the correlation, a destructive failure analysis was performed after the TS cycling. The cross-sectional images along line 1-1 of $MC1_1$ are shown in Fig. 10. The images show clearly cracks at all three interfaces (molding compound/copper pad, silicon die/die attach, and die attach/copper pad), which validates the SAM investigation. The cross-sectional images along line 2-2 of $MC1_1$ are shown in Fig. 10. The images clearly indicate the presence

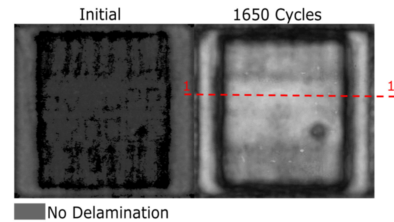

Fig. 11. SAM of $MC1_2$ in discrete time. No delamination is present and one cross section is performed at the end of the experiment.

of cracks at all three interfaces. The images also confirm the interface with no delamination that the SAM images were able to identify.

In the case of TV $MC1_2$, there was no significant change in stresses during the experiment, indicating that no delamination occurred. This is confirmed by the SAM images obtained after the experiment (see Fig. 11). It was further corroborated by the cross-sectional images.

V. Diagnostics

Diagnostics consists of two steps: fault detection by Mahalanobis distance (MD) and fault clarification by a clustering technique.

A. Fault Detection

Fault detection by MD was described in detail for fault classification in [8] and for fault detection in [10] and [24]. MD is the distance between a point and a distribution, and not between two distinct points, like Euclidean distance. It is effectively a multivariate equivalent of the Euclidean distance. Basically, it is the normalized distance between the test point from the sample mean over the SD. A healthy baseline and a threshold are needed to classify the product states (healthy or unhealthy). They are determined by the well-known MD. The methodology begins with gathering the sensor data, i.e., the values of stress difference at 480 sensor cells. These values are referred to as performance parameters. They are stored in a matrix X_{ij} with elements denoted as xij, where $i = 1, 2, \ldots, p$ and p is the total number of performance parameters (here, $p = 480$) and $j = 1, 2, \ldots, m$, where m is the total number of MPs. A representative MD applied to the stress sensor cells is shown in Fig. 12. The healthy baseline is created on the first 800 MPs of no delamination. The data points exceeding the failure limit are clearly seen in the MD results after 850 cycles, where delamination occurred. The failure detection point is defined. The threshold was computed from the healthy data (i.e., no initial delamination). The result is also plotted in Fig. 12.

Since the MD is not normally distributed, a Box Cox transformation [25] is used to convert the data into a normal distribution. A warning limit threshold is defined as $(\mu + 2\sigma)$ and a fault alarm threshold as $(\mu + 3\sigma)$, based on the normal distribution parameters. A limitation of the MD is found that the healthy baseline cannot be updated.

Authorized licensed use limited to: University of Maryland College Park. Downloaded on March 07,2022 at 11:42:47 UTC from IEEE Xplore. Restrictions apply.

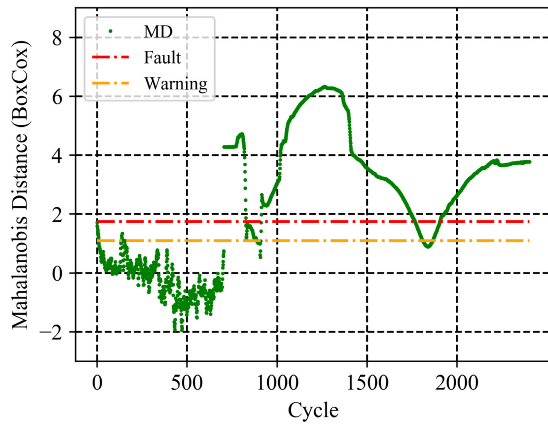

Fig. 12. Classic threshold MD applied to TQFP stress sensor data. The fault is detected around 850 cycles.

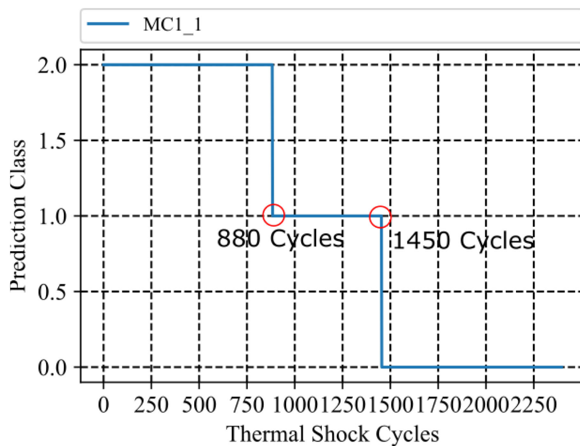

Fig. 13. Prediction class with k-means clustering method. On prediction class axis 2 represents the health state, 1 represents the delamination between the molding compound and the copper pad, and 0 represents delamination between the adhesive and the silicon die.

TABLE II
CONTOUR PLOT STANDARD DEVIATION

Input: Stress Difference $D(\sigma)_{ijk}$, Cycle Interval
Output: Standard Deviation SD_{ijl} per Interval

Step 1. Calculate the average of each column:
$\bar{x_{ij}} = \frac{1}{r}\sum_{l=1}^{r} D(\sigma)_{ij}$
Step 2. Calculate the standard deviation:
$SD_{ij} = \sqrt{\frac{\sum_{l=1}^{r}(D(\sigma)_{ij} - \bar{x_{ij}})^2}{r-1}}$
Step 3. Plot the contour matrix SD_{20x24}.
Step 4. Evaluate the crack tip on the contour plot.

$*i = 1, 2, ..., n$ and $n = 20$ number of cells in x direction
$*j = 1, 2, ..., m$ and $m = 24$ number of cells in y direction
$*k = 1, 2, ..., p$ and $p =$ number of cycles
$*l = 2, ..., r$ and $r =$ Cycle Interval where standard deviation is calculated

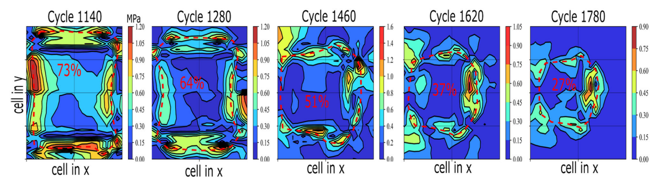

Fig. 14. Stress difference SD every 20 cycles plotted on a contour image for $MC1_1$. The crack tip is given by the high SD.

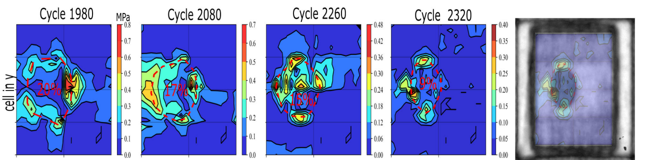

Fig. 15. Stress difference SD every 20 cycles plotted on a contour image for $MC1_1$. The crack tip is given by the high SD. This is validated over the SAM images on this TV, but also on the other TVs.

B. Fault Classification

One way of classifying the data is *clustering*, which is a common unsupervised ML technique. Its aim is to divide objects into groups according to the distance-based similarity measure [26]. This method is chosen because of its computational effectiveness among other unsupervised ML methods. A clustering technique is used to classify the data. To reveal hidden information such as the necessary number of clusters, the Elbow method, described in [26], is used. All the 480 stress sensing cells are used in the algorithm. Based on the elbow method, only three clusters are needed to correctly split the data. Based on the number of prediction class outputs and the previous knowledge from failure analysis, three subgroups are identified. This can be visualized in Fig. 13, as follows: the first subgroup is the healthy class 2 until 880 TS cycles; the second subgroup is the data associated with the delaminated copper pad/molding compound interface; and the third subgroup contains the data obtained after 1450 cycles onward attributed to the delamination at the adhesive/silicon die interface.

The results from the clustering are an indirect validation of the assumption in Section IV that delamination starts at the outer areas of the silicon die, resulting in an increase in the stress difference.

C. Fault Location

As depicted in Fig. 3, the silicon die consists of 20 sensing cells in the x-direction and 24 cells in the y-direction. It is observed that a high value of the SD per each r number of interval cycles corresponds to the crack tip location in the adhesive layer. The steps followed in calculation of the SD are described in Table II.

For this case, an interval of 20 cycles is chosen to evaluate the SD. This value is chosen to have an effective number of pictures that needs to be manually evaluated. Some of them are depicted in Figs. 14 and 15. It is clearly shown that the high values of SD in the contour plot correspond to the crack tip in the adhesive layer. This way, it is possible to follow the crack tip delamination area at least every two cycles.

Authorized licensed use limited to: University of Maryland College Park. Downloaded on March 07,2022 at 11:42:47 UTC from IEEE Xplore. Restrictions apply.

In Fig. 15, an SD contour plot image is overlaid over the SAM image. This corroborates with our observation that the high values of SD indicate the location of the crack tip. This validation is performed on all the other SAM images available and validates our observations.

Every image is then manually evaluated, and a red-dotted path is drawn over the high values of the SD. The area formed inside the path is then divided by the total area of the sensor area and transformed into percentage. Therefore, at least every two cycles, an estimated remaining not delaminated area can be manually evaluated.

VI. Health Assessment and Prognostics

A. Degradation Estimation

Echo state network (ESN) is a new type of recurrent neural network (RNN) proposed in recent years and was developed by Jaeger [27]. The training process of the ESN is easier and less computationally intensive than the regular RNN, which has the same size [28].

RUL is the amount of time left before a system fails to operate within acceptable limits. RUL calculation is similar to time-to-failure calculation, except that an upper operating limit threshold is used instead of a failure threshold [29]. Defining a degradation threshold for RUL is a challenging task as it strictly depends on applications. Various application-specific integrated circuits (ASICs) can be packaged in the same type of the housing, such as TQFP. For an application with relatively small power dissipation (below 1 W), only 10% of the die attach contact area can still provide good functionality of the ASIC, while for other application with larger power dissipation, even 20% of the contact area can bring the device to an end of life. In our study, we have assumed 10% of the contact area as a threshold for an end of life, i.e., a good connection between the silicon die and the die paddle is assumed to be provided even after 90% of the die attach is delaminated. It is to be noted that the threshold value should be adjusted for different applications. In this article, the ESN method is used for the estimation and prediction of degradation based on incremental stress values. The RUL is predicted by extrapolation from the degradation estimation. For the purpose RUL calculation, the degradation grades of "complete delamination" and "no delamination" are set to be 0% and 100%, respectively. Half of the data from TVs $MC1_1$, $M2_1$, and $M2_4$ are used for both the training set and the testing set. The data from $M1_2$,, $M2_2$, and $M2_3$ are used for the analysis. In a real-time prognosis, the inputs are the stress difference of that specific point in time, and the output will be the degradation estimation percentage. The input of the ESN is defined as all relative stresses $D(\sigma)$ of all valid MPs in all sensors as

$$u = D(\sigma)_{ij} \tag{4}$$

where $i = 1, 2, \ldots, n$ and n is the total number of cells (480 in this case), and $j = 1, 2, \ldots, m$ and $m =$ number of cycles.

The output of the ESN defined as the degradation grade is a function from 100% to 0% created based on the SD values. This evaluation is performed manually on the contour plot image

TABLE III
Range of Parameters of the RNN [30]

Parameter	Commonly used range
Reservoir size	[50,800]
Spectral radius	[0.1,1)
Input scaling	[0,1]
Input shift	$[0,\max_{input}]$
Output scaling	[0,1]
Output shift	$[0,\max_{output}]$

every 20 cycles. This is a time-consuming task and, therefore, needs to be automated. Training half of the TVs' data is an attempt to generalize the model. The rest of TVs' data are evaluated by the model, without being necessary to manually evaluate the delamination area based on the fault location

$$y = \begin{pmatrix} 100\% \\ \frac{R_1}{N} \times 100\% \\ \frac{R_2}{N} \times 100\% \\ \vdots \\ \frac{R_n}{N} \times 100\% \\ 0\% \end{pmatrix} \tag{5}$$

where R is the area evaluated by manually drawing a red-dotted path and N is the total area of the physical sensor.

Data from three TVs $MC1_1$, $M2_1$, and $M2_4$ were used to train the network. Cross-validation was used in the training process that involved the separation of data into k folds. In this study, $k = 10$ was used. After the division, the model was trained on nine of these folds and then was subsequently validated using the remaining fold. The average of the ten measures mean square error (MSE) was the metric used to improve the model.

Up to the point where there is a failure detected, the output is considered 100% as of no delamination is present. Afterward, a manually created function is used to describe the degradation [see (5)].

The parameter size of dynamic reservoir n, the desired spectral radius of dynamic reservoir r, the input shift and scaling, and the output shift and scaling have to be optimized. Table III shows the commonly used range of parameters.

The optimization strategy used in this case is a conservative one. Change one parameter with a certain step, keep others unchanged, and train the ESN using the cross-validation to get the lowest MSE.

During optimization, the ESN was trained and tested for 10^6 times. The minimum MSE was then found, and its combination of parameter was recorded. The optimization process took about 5 h. From this optimization, it is observed that the reservoir size and the spectral radius are two main factors influencing MSE. A very good practical guideline can be found in [31]. The execution time of the model is 659 ms for fitting and 745 ms for prediction; degradation prediction in percentage for all the testing modules is shown in Fig. 16. Degradation percentages here refer to delamination area. Comparing the results from the

Authorized licensed use limited to: University of Maryland College Park. Downloaded on March 07,2022 at 11:42:47 UTC from IEEE Xplore. Restrictions apply.

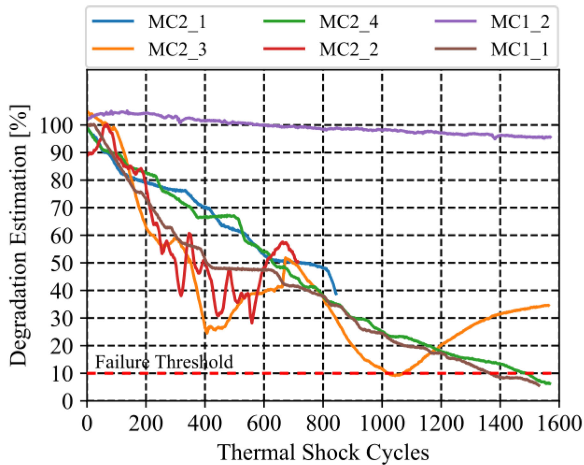

Fig. 16. Degradation estimation ESN output for $MC1$ and $MC2$.

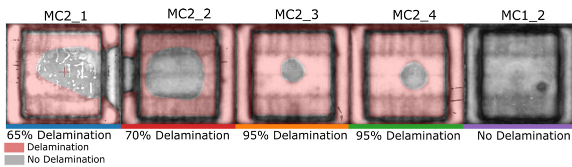

Fig. 17. SAM images at the end of the experiments for $MC1$ and $MC2$.

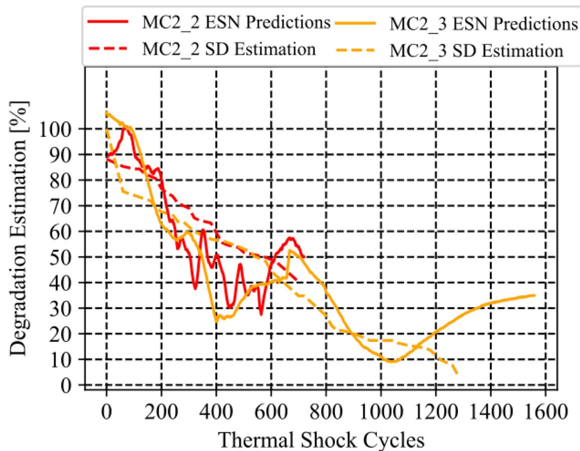

Fig. 18. Degradation estimation ESN output versus SD estimation.

ESN prediction and the SAM images from Fig. 17, the following can be stated.

1) For TVs $MC2_1$ and $MC2_2$, a 30% delamination area remaining is predicted by the ESN. This is validated by the SAM images.
2) For TVs $MC2_3$ and $MC2_4$, the model predicts an almost full delamination percentage close to few percentages. This is also confirmed by the SAM images.
3) As expected for TV $MC1_2$, no degradation is predicted.

Following the same methodology from the fault location section, the degradation estimation for the other TVs was also evaluated and is depicted in Fig. 18. A comparison between the ESN model and the SD methodology is shown. The results shows good accuracy in generalization of the ESN model. The model can be, of course, improved by including more samples data into the training data.

Based on the neural network model, RUL estimation can be extrapolated. However, how to extrapolate RUL from this model under real operating conditions still remains a challenge that must be addressed in the future studies. It is observed that the RUL for all the modules strongly depends on the failure detection point, loading conditions, and material properties.

VII. Conclusion

In this article, the thermomechanical stress-based prognostics approach was developed to extend the stress-based PHM capability into a quantitative domain, where accurate prediction of RUL became possible. The approach was implemented with actual microelectronics packages subjected to harsh accelerated testing conditions. Piezoresistive stress sensors were employed to measure the internal stresses of microelectronic packages. An AU and a Raspberry Pi were used for sensor data read-out, collection, and evaluation. Accelerated tests in a thermal convection chamber were performed, and the resultant failure data were utilized to conduct data processing. The statistical techniques for diagnostics and the ML algorithms for health assessment and prognostics were then implemented to estimate and predict the degradation state.

The neural network model used in this article was built and tested by using one half of TVs as a training set and the other half of TVs as a testing set. The network parameters were optimized only for these datasets. More datasets must be obtained to train and test the network so that a more generalized model can be created. Nevertheless, the results show that the proposed framework and approach outperforms the conventional failure analysis approach (e.g., SAM analysis). The results also confirm that data-driven approaches provide the opportunity not only to monitor the asset during operation, but also to understand the asset behavior based on its current design. This can lead to a better product in the future and to further optimize resources and expenditures.

References

[1] W.-S. Lei and A. Kumar, "Delamination and reliability issues in packaged devices," in *Adhesion in Microelectronics*, K. Mittal and T. Ahsan, Eds., Hoboken, NJ, USA: Wiley, 2014, pp 267–312.

[2] G. Q. Zhang, W. D. V. Driel, and X. J. Fan, *Mechanics of Microelectronics (Solid Mechanics and Its Applications Series)*, vol. 141. New York, NY, USA: Springer, 2006.

[3] N. Vichare and M. Pecht, "Prognostics and health management of electronics," *IEEE Trans. Compon. Packag. Technol.*, vol. 29, no. 1, pp. 222–229, Mar. 2006.

[4] Y. Zou, J. C. Suhling, R. W. Johnson, and R. C. Jaeger, "Complete stress state measurements in chip on board packages," in *Proc. Int. Conf. Multichip Modules High Density Packag.*, 1998, pp. 405–415

[5] A. R. R. Adli, K. M. B. Jansen, F. Schindler-Saefkow, and F. Rost, "Experimental investigation and interpretation of the real time, in situ stress measurement during transfer molding using the piezoresistive stress chips," in *Proc. 15th Int. Conf. Thermal, Mech. Multi-Phys. Simul. Exp. Microelectron. Microsyst.*, 2014, pp. 1–4.

Authorized licensed use limited to: University of Maryland College Park. Downloaded on March 07,2022 at 11:42:47 UTC from IEEE Xplore. Restrictions apply.

[6] Y. Zou, J. C. Suhling, R. W. Johnson, R. C. Jaeger, and A. K. M. Mian, "In-situ stress state measurements during chip-on-board assembly," *IEEE Trans. Electron. Packag. Manuf.*, vol. 22, no. 1, pp. 38–52, Jan. 1999.

[7] A. Palczynska, P. J. Gromala, D. Mayer, B. Han, and T. Melz, "In-situ investigation of EMC relaxation behavior using piezoresistive stress sensor," *Microelectron. Rel.*, vol. 62, pp. 58–62, 2016.

[8] A. Prisacaru, A. Palczynska, A. Theissler, P. Gromala, B. Han, and G. Q. Zhang, "*In situ* failure detection of electronic control units using piezoresistive stress sensor," *IEEE Trans. Compon. Packag. Manuf. Technol.*, vol. 8, no. 5, pp. 750–763, May 2018.

[9] B. Wu, D.-S. Kim, B. Han, A. Palczynska, A. Prisacaru, and P. J. Gromala, "Hybrid approach to conduct failure prognostics of automotive electronic control unit using stress sensor as in situ load counter," *IEEE Trans. Compon. Packag. Manuf. Technol.*, vol. 9, no. 1, pp. 28–38, Jan. 2019.

[10] A. Palczynska, A. Prisacaru, P. J. Gromala, B. Han, D. Mayer, and T. Melz, "Towards prognostics and health monitoring: The potential of fault detection by piezoresistive silicon stress sensor," in *Proc. 17th IEEE Int. Conf. Thermal, Mech. Multi-Phys. Simul. Exp. Microelectron. Microsyst.*, 2016, pp. 1–8.

[11] A. Prisacaru, A. Palczynska, P. J. Gromala, B. Han, and G. Q. Zhang, "*Condition monitoring algorithm for piezoresistive silicon-based stress sensor data obtained from electronic control units*," *Proc. IEEE 67th Elect. Compon. Technol. Conf.*, 2017, pp. 1119–1127.

[12] F. Schindler-Saefkow *et al.*, "Stress chip measurements of the internal package stress for process characterization and health monitoring," in *Proc. 13th Int. Thermal, Mech. Multi-Phys. Simul. Exp. Microelectron. Microsyst.*, 2012, pp. 1/ 10–10/10.

[13] M. K. Rahim, J. C. Suhling, R. C. Jaeger, and P. Lall, "Fundamentals of delamination initiation and growth in flip chip assemblies," in *Proc. Electron. Compon. Technol., 2005,* pp. 1172–1186.

[14] A. Prisacaru, E. O. Guerrero, P. J. Gromala, B. Han, and G. Q. Zhang, "Degradation prediction of electronic packages using machine learning," in *Proc. 20th Int. Conf. Thermal, Mech. Multi-Phys. Simul. Exp. Microelectron. Microsyst.*, 2019, pp. 1–9.

[15] A. Prisacaru, A. Palczynska, P. Gromala, B. Wu, B. Han, and G. Zhang, "Accuracy of CMOS-based piezoresistive stress sensor for engineering applications of thermal loading condition: Theoretical review and experimental validation," *IEEE Sens. J.*, vol. 19, no. 20, pp. 9139–9148, Oct. 2019.

[16] R. Jaeger, J. Suhling, R. Ramani, A. Bradley, and J. Xu, "CMOS stress sensors on [100] silicon," *IEEE J. Solid-State Circuits*, vol. 35, no. 1, pp. 85–95, Jan. 2000.

[17] R. B. GmbH, "Abschlussbericht zum verbundvorhaben iforcesens: Entwicklung eines integrierten stressmesssystems zur quantifizierung der 3 d-v erformung von sensorbauelementen in abhangigkeit des verpackungsprozesses," Technische Informationsbibliothek, 2008. [Online]. Available: https://doi.org/10.2314/GBV:606643435

[18] H. Kittel, S. Endler, H. Osterwinter, S. Oesterle, and F. Schindler-Saefkow, "Novel stress measurement system for evaluation of package induced stress," in Proc. 2nd Eur. Conf. Exhib. Integr. Issues Miniaturized Syst.—MOMS, MOEMS, ICS, Electron. Compon., 2008, pp. 1–8.

[19] A. Palczynska, F. Pesth, P. J. Gromala, T. Melz, and D. Mayer, "Acquisition unit for in-situ stress measurements in smart electronic systems," in *Proc. 15th IEEE Int. Conf. Thermal, Mech. Multi-Phys. Simul. Exp. Microelectron. Microsyst*., 2014, pp. 1–4.

[20] S. Naduvil-Vadukootu, R. Angryk, and P. Riley, "Evaluating preprocessing strategies for time series prediction using deep learning architectures," 2017. [Online]. Available: https://aaai.org/ocs/index.php/FLAIRS/FLAIRS17/paper/view/15475

[21] S. A. Alasadi and W. S. Bhaya, "Review of data preprocessing techniques in data mining," *J. Eng. Appl. Sci.*, vol. 12, no. 16, pp. 4102–4107, 2017.

[22] Y.-H. Yang, B. Han, A. Prisacaru, P. Gromala, S. Jiang, and A. Sarwar, "In-situ service load monitoring of automotive electronic systems using silicon-based piezoresistive stress sensor," *Microelectron. Rel.*, vol. 110, Jul. 2020, Art. no. 113650.

[23] A. Inamdar *et al.*, "Study of thermal aging behavior of epoxy molding compound for applications in harsh environments," in *Proc. IEEE 69th Electron. Compon. Technol. Conf.*, 2019, pp. 811–818.

[24] S. Kumar, T. Chow, and M. Pecht, "Approach to fault identification for electronic products using Mahalanobis distance," *IEEE Trans. Instrum. Meas.*, vol. 59, no. 8, pp. 2055–2064, Aug.2010.

[25] M. Pecht, "Prognostics and health monitoring of electronics," in *Proc. IEEE Int. Conf. Electron. Mater. Packag.*, 2006, pp. 1–10.

[26] F. Pedregosa *et al.*, "Scikit-learn: Machine learning in python," *J. Mach. Learn. Res.*, vol. 12, pp. 2825–2830, 2011.

[27] H. Jaeger, "Harnessing nonlinearity: Predicting chaotic systems and saving energy in wireless communication," *Science*, vol. 304, no. 5667, pp. 78–80, Apr. 2004.

[28] J. Dai, G. K. Venayagamoorthy, and R. G. Harley, "An introduction to the echo state network and its applications in power system," in *Proc. 15th Int. Conf. Intell. Syst. Appl. Power Syst.*, Nov. 2009, pp. 1–7.

[29] D. Galar, U. Kumar, J. Lee, and W. Zhao, "Remaining useful life estimation using time trajectory tracking and support vector machines," *J. Phys.: Conf. Ser.*, vol. 364May 2012, Art. no. 012063.

[30] E. Z. Marco Rigamonti and P. Baraldi, Echo state network for the remaining useful life prediction of a turbofan engine," in *Proc. Eur. Conf. Prognostics Health Manage. Soc.*, vol. 3, no. 1, Jul. 2016.

[31] M. Lukosevicius, "A practical guide to applying echo state networks," in *Neural Networks: Tricks of the Trade*. Berlin, Germany: Springer, 2012.

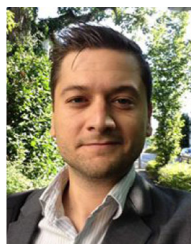

Alexandru Prisacaru received the master's degree in computational engineering from the Ruhr University of Bochum, Bochum, Germany, in 2015, and the master's degree in structural engineering from Technical University "Gheorghe Asachi," Iaşi, Romania, in 2011. He is currently working toward the Ph.D. degree with the Division of Automotive Electronics, Robert Bosch GmbH, Reutlingen, Germany.

His Ph.D. work is performed in cooperation with the "Micro/Nanoelectronics System Integration and Reliability" Department, Delft University of Technology, Delft, The Netherlands. His research interests include developing and implementing prognostics and health management techniques of relevant electronics for future autonomous driving applications. Among these, his technical expertise include computational structural mechanics, material modeling, statistical pattern recognition, machine learning methods, and surrogate modeling.

Przemyslaw Gromala (Senior Member, IEEE) received the Ph.D. degree in mechanical engineering from the Cracow University of Technology, Kraków, Poland, in 2010.

He is currently a Simulation Senior Expert with the Division of Automotive Electronics, Robert Bosch GmbH, Reutlingen, Germany, where he is currently leading an international simulation team and finite-element method verification laboratory with the main focus on implementation of simulation driven design for electronic control modules and multichip power packaging for hybrid drives. His research interests include virtual prequalification techniques for development of the electronic control modules and multichip power packaging. His technical expertise include material characterization and modeling and multidomain and multiscale simulation including fracture mechanics, verification techniques, and prognostics and health monitoring for future-safety-related electronic smart systems. Prior to joining Robert Bosch GmbH, he worked at Delphi Development Center, Kraków, as well as at Infineon Research and Development Center, Dresden, Germany.

Dr. Gromala is an Active Committee Member of the IEEE Electronic Components and Technology Conference, the International Conference on Thermal, Mechanical and Multi-Physics Simulation and Experiments in Microelectronics and Microsystems, the International Conference on Electronic Packaging Technology, and the International Electronic Packaging Technical Conference and Exhibition. He is also an Active Committee Member of the European Technology Platform on Smart Systems Integration, which is an industry-driven policy initiative defining R&D and innovation needs as well as policy requirements related to smart systems integration and integrated micro- and nanosystems.

Authorized licensed use limited to: University of Maryland College Park. Downloaded on March 07,2022 at 11:42:47 UTC from IEEE Xplore. Restrictions apply.

Bongtae Han received the B.S. and M.S. degrees in mineral and petroleum engineering from Seoul National University, Seoul, South Korea, in 1981 and 1983, respectively, and the Ph.D. degree in engineering mechanics from Virginia Tech, Blacksburg, VA, USA, in 1991.

He is currently a Keystone Professor of Engineering and APT Chair of the Mechanical Engineering Department, University of Maryland, College Park, MD, USA, where he is currently directing the Laboratory for Optomechanics and Micro/Nano Semiconductor/Photonics Systems, Center for Advanced Life Cycle Engineering. He has coauthored a text book entitled *High Sensitivity Moiré: Experimental Analysis for Mechanics and Materials* (New York, NY, USA: Springer-Verlag, 1997) and edited two books. He has authored or coauthored 12 book chapters and more than 250 journal and conference papers in the field of microelectronics, photonics, and experimental mechanics. He holds two U.S. patents and four invention disclosures.

Dr. Han received the IBM Excellence Award for Outstanding Technical Achievements in 1994. He was a recipient of the 2002 Society for Experimental Mechanics (SEM) Brewer Award for his contributions to development of photomechanics tools used in semiconductor packaging and the 2016 American Society of Mechanical Engineering (ASME) Mechanics Award in Electronic and Photonic Packaging Division for his contributions to structural mechanics of electronic systems. He was also the recipient of the Best Paper Award of the IEEE TRANSACTIONS ON COMPONENTS AND PACKAGING TECHNOLOGIES in 2004, the Gold Award (Best Paper in the Analysis and Simulation Session) at the 1st Samsung Technical Conference in 2004, and the Best Paper Award at the 16th International Conference on Electronic Packaging Technology in 2015. He was an Associate Technical Editor for *Experimental Mechanics* from 1999 to 2001 and the *Journal of Electronic Packaging* from 2003 to 2012. He is an Associate Editor for *Microelectronics Reliability*. He became a Fellow of the SEM and the ASME in 2006 and 2007, respectively.

Guo Qi Zhang (Fellow, IEEE) received the Ph.D. degree in aerospace engineering from the Delft University of Technology (TU Delft), Delft, The Netherlands, in 1993. He was with Philips, Amsterdam, The Netherlands, for 20 years as a Principal Scientist from 1994 to 1996, the Technology Domain Manager from 1996 to 2005, the Senior Director of Technology Strategy from 2005 to 2009, and a Philips Fellow from 2009 to 2013. He also had part-time appointments as a Professor at the Technical University of Eindhoven from 2002 to 2005, and as a Chair Professor at the Delft University of Technology (TU Delft) from 2005 to 2013.

Prof. Zhang serves as the Deputy Director of the European Center for Micro- and Nanoreliability, a Co-Chair of the Advisory Board of the International Solid State Lighting Alliance, and the Secretary General of the International Technology Roadmap of Wide Band Gap Semiconductors. He chaired the Eniac Strategic Research Agenda team of More than Moore and served as a Co-Chair of the Academic Council of the Dutch National Innovation Program on Micro/Nanoelectronics and Embedded System.

Authorized licensed use limited to: University of Maryland College Park. Downloaded on March 07,2022 at 11:42:47 UTC from IEEE Xplore. Restrictions apply.